Activation Analysis for LHD Experiments with Deuterium Gases

Kiyohiko Nishimura, Hirokuni Yamanishi and Akio Komori

National Institute for Fusion Science, 322-6 Oroshi-cho, Toki 509-5292, Japan

Identification of radionuclides and evaluation of dose rate level have been carried out on the structural materials of the Large Helical Device and the Experimental Hall. The neutron fluence was calculated using two-dimensional transport code DOT-3.5. Energies of neutron sources are 2.45 MeV (D-D reaction) and 14 MeV (D-T reaction). Generations of radionuclides were calculated using CINAC code. Radionuclides of ^{93m}Nb, ^{63}Ni and ^{60}Co for helical coils, ^{55}Fe and ^{60}Co for stainless steel, ^{55}Fe, ^{60}Co and ^{93m}Nb for poloidal coils, ^{40}K and ^{55}Fe for floor concrete were dominant after a series of experiments with deuterium gases. Evaluation of dose rate level for the structural materials and air were calculated taking account a present experimental schedule.

Keywords: Large Helical Device, deuterium operation, Superconducting coils, radioactivity, dose rates, DOT-3.5 code, CINAC code, cobalt 60

1. Introduction

In fusion devices such as JT-60U, TFTR and JET neutron production generated by deuterium-deuterium reactions is increased accompany with the increase in fusion power and the devices are subsequently activated. As a result, maintenance and repair works during off-operational periods become difficult because an access around and/or into a vacuum vessel is so limited from a health physics point of view. A safety analysis is also a major concern of experiments with deuterium gases in the Large Helical Device (LHD) [1-4] and a design of DEMO reactors with high neutron yield operations.

Several calculations concerning induced activities for the tokamak devices have been reported. In these tokamaks, varied structural materials are used so that characteristics of radioactivity differ with each device. For this reason, it is clear that information of inherent property of activation on LHD is essential to an understanding of the dose rate around the device in maintenance works.

The radiation protection concepts of the LHD was carried out at the building design phase [5] and revised at the building construction phase [6]. The neutron fluence was calculated using two-dimensional transport code DOT-3.5 [7]. Generations of radionuclides caused by 2.45 MeV (D-D reaction) and 14 MeV (D-T reaction) were calculated using CINAC code [8].

In this paper, identification of radionuclides and evaluation of the dose rate on the LHD are described.

2. Large Helical Device

LHD is the largest superconducting heliotron type device with l=2/m=10 continuous helical coils and three pairs of poloidal coils. The major and minor radii of the plasma are 3.5-3.9 m and 0.6-0.65 m, respectively. Schematic figure of LHD are shown in Fig. 1. The maximum magnetic field strength is about 3 T at the magnetic axis.

The LHD project is aimed at exploring the feasibility of helical plasmas for fusion applications. In particular, to demonstrate the steady-state currentless plasmas confined in the helical fields generated by super-conducting coils.

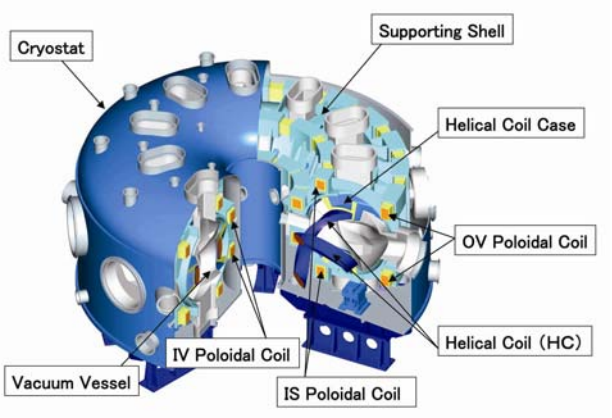

Fig. 1. Schematic figure of LHD.

author's e-mail: nisimura@LHD.nifs.ac.jp

3. Calculation

Standard numbers and energies of neutron sources using calculations are shown in Table 1. One shot is 10 seconds pulse and 1000 shots are operated in a year.

Table 1. Parameters of neutron

Energy (MeV)	Number (1/shot)
2.45	2.4×10^{17}
14.0	4.3×10^{15}

The most of 2.45MeV neutrons (D-D neutron) are generated by D plasma and D^0 beam reaction, which is called TCT effect. The14.0 MeV neutrons (D-T neutron) are generated by the reaction of deuterium with tritium (1.01 MeV) through D-D reaction. The number of D-D thermonuclear reaction is 1 – 3 % of that of TCT effect.

The neutron fluence data and the distribution of γ-ray were calculated using two-dimensional transport code DOT-3.5 by means of the FUSION-40 nuclear data set [9]. Generations of radionuclides were calculated using CINAC code. Effects of chain disintegration were taking account in this code. Since the LHD has three-dimensional structure, it is difficult to model this geometry on a two-dimensional configuration. Two models (a horizontal port model and a vertical port model) with R-Z geometry were used in these calculations. Figure 2 shows cross sections of these two models near the LHD. Calculated area was divided into twelve regions; plasma, helical coil, helical coil case, supporting shell, IV poloidal coil, IS poloidal coil, OV poloidal coil, cryostat, vacuum vessel, wall and ceiling concrete, floor concrete and air. LHD experimental hall has 45m x 75m of floor area and 40m of height. Thickness of walls and floor concrete is 2m and thickness of ceiling concrete is 1.3m. In R-Z model calculation, R of 2.5m and Z of 40m were assumed.

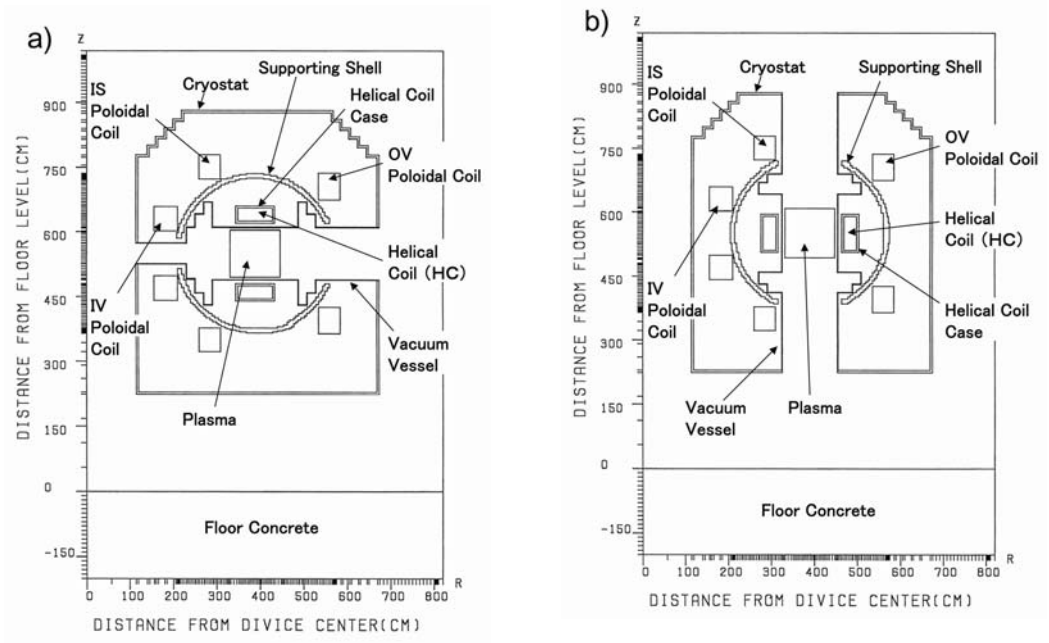

Fig. 2. Cross sections of models.
a) vertical port model, b) horizontal port model.

4. Results

Detail analysis was carried out to identify the radionuclides, which give the contribution to the γ-ray dose rate, and to calculate time evolution of the dose rate after a stop of D-D experiments.

Figures 3 and 4 show results of specific radionuclide activities as a function of time after 1 shot pulse. Two figures show averaged activities of the cryostat (SS-316) and the floor concrete. In the cryostat, ^{56}Mn (half-life of 2.6h) generated by a reaction of ^{55}Mn(n,γ) is dominant by the time of one day. After disappearance of ^{56}Mn, ^{51}Cr (27.7d) becomes dominant. After that, ^{60}Co (5.27y) generated by a reaction of ^{59}Co(n,γ) becomes dominant. In floor concrete, many radionuclides with short half-life are dominant by the time of one day. After disappearance of these shot life time nuclides, ^{24}Na (15.0h) generated by a reaction of ^{23}Na(n,γ) becomes dominant for a week. After that, ^{40}K (1.28×10^9y) becomes dominant. Most of the ^{40}K are nuclides naturally existing in a concrete.

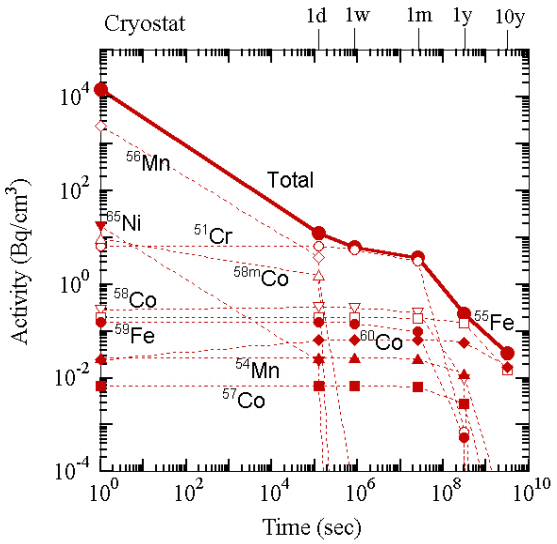

Fig. 3. Specific activity in the Cryostat (SS316) after 1 shot.

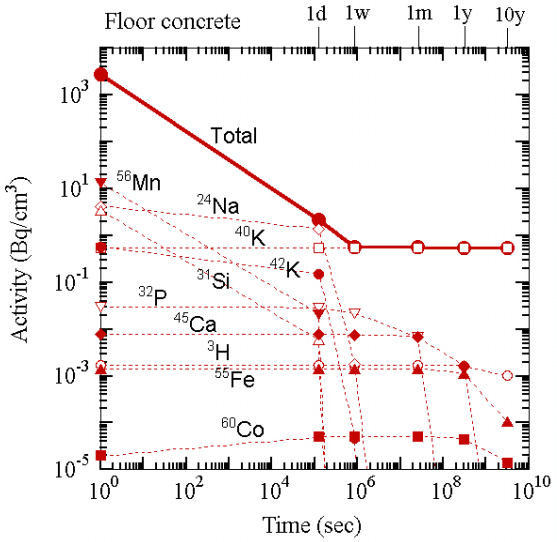

Fig. 4. Specific activity in the floor concrete after 1 shot.

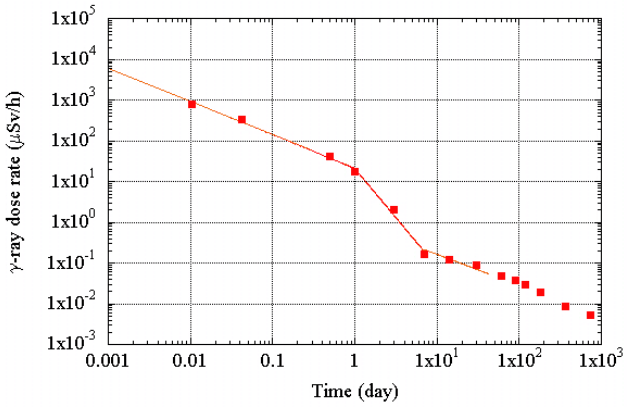

Fig. 5. Time evolution of total γ-ray dose rate after 3 seconds pulse.

To estimate the γ-ray dose rate around the vacuum vessel, total dose by all structural materials was calculated at the front of L-port of LHD. Figure 5 shows this result. In this calculation, actual experimental plan were used; 3 seconds pulse in each 15 minutes, 30 shots in a day, 4 days in a week, 3 weeks experiment and 3 weeks intermission. Using this curve, time evolution of γ-ray dose rate during experimental series was calculated by summing up contributions of each shot. Figure 6 shows a result of one experimental series. During three days in weekend, the γ-ray dose rate decreases one order. This level of 10μSv/h is lower than the limitation for worker (20mSv/y) who works for 2000 hours per year.

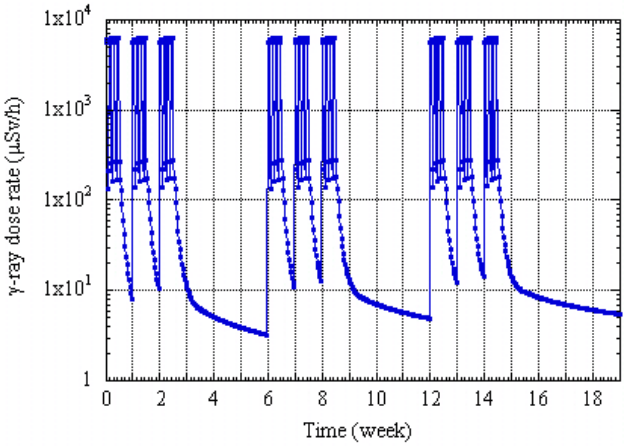

Fig. 6. Time evolution of γ-ray dose rate during experimental series.

Table 2-1. Activities of typical radionuclides on stainless steel structures 1.

Activities of typical radionuclides on stainless-steel 1.

after 1000 shots
horizontal port model

Volume (cm^3)	
VV	6.08E+06
HC Case	5.88E+06

radio-nuclides	Vacuum Vessel		HC Case	
	after 1year (Bq/cc)	after 10years (Bq/cc)	after 1year (Bq/cc)	after 10years (Bq/cc)
Be-10	3.97E-09	3.97E-09	1.88E-09	1.88E-09
C-14	1.27E-02	1.26E-02	1.83E-02	1.82E-02
Si-32	9.28E-11	9.20E-11		
P-32	4.39E-07	9.20E-11	5.23E-07	
P-33	2.93E-06			
S-35	1.29E-04			
Cr-51	1.08E-02		5.63E-03	
Mn-53	1.25E-05	1.25E-05	6.26E-06	6.26E-06
Mn-54	2.39E+02	1.62E-01	1.34E+02	9.08E-02
Fe-55	4.21E+02	4.12E+01	5.57E+02	5.46E+01
Fe-59	1.01E+00		2.17E+00	
Fe-60	7.31E-10	7.31E-10	3.46E-10	3.46E-10
Co-56	2.01E-03		9.52E-04	
Co-57	5.49E+01	1.25E-02	2.69E+01	6.12E-03
Co-58	2.44E+02	2.89E-12	1.38E+02	1.77E-12
Co-60	8.80E+01	2.70E+01	2.34E+02	7.16E+01
Ni-59	2.26E-02	2.26E-02	5.58E-02	5.58E-02
Ni-63	1.54E+00	1.45E+00	5.79E+00	5.44E+00
Zr-93	2.69E-08	2.69E-08	1.40E-08	1.40E-08
Zr-95	4.42E-03		2.27E-03	
Nb-95m	4.22E-05		2.16E-05	
Nb-94	1.21E-05	1.21E-05	6.16E-06	6.16E-06
Nb-95	1.11E-02		5.72E-03	
Nb-93m	4.23E-05	3.39E-04	2.17E-05	1.74E-04
Mo-93	9.45E-04	9.43E-04	4.86E-04	4.85E-04
Tc-99	1.47E-03	1.47E-03	2.55E-03	2.55E-03

Table 2-2. Activities of typical radionuclides on stainless steel structures 2.

Activities of typical radionuclides on stainless-steel 2.

after 1000 shots
horizontal port model

Volume (cm^3)	
SS	2.33E+07
Cryostat	2.71E+07

radio-nuclides	Supporting Shell		Cryostat	
	after 1year (Bq/cc)	after 10years (Bq/cc)	after 1year (Bq/cc)	after 10years (Bq/cc)
Be-10	5.53E-10	5.53E-10	1.25E-10	1.25E-10
C-14	5.95E-03	5.95E-03	4.46E-03	4.46E-03
Si-32			5.16E-12	5.11E-12
P-32	1.95E-07		1.53E-07	5.11E-12
P-33			3.68E-07	
S-35			1.85E-04	
Cr-51	1.61E-03		3.41E-04	
Mn-53	1.76E-06	1.76E-06	3.66E-07	3.66E-07
Mn-54	4.25E+01	2.87E-02	8.73E+00	5.91E-03
Fe-55	2.02E+02	1.98E+01	1.17E+02	1.15E+01
Fe-59	8.92E-01		4.62E-01	
Fe-60	1.00E-10	1.00E-10	1.43E-11	1.43E-11
Co-56	2.75E-04		3.93E-05	
Co-57	7.93E+00	1.80E-03	1.15E+00	2.63E-04
Co-58	4.78E+01	5.59E-13	6.92E+00	8.22E-14
Co-60	7.20E+01	2.21E+01	5.01E+01	1.53E+01
Ni-59	1.52E-02	1.52E-02	9.64E-03	9.64E-03
Ni-63	9.90E-01	9.30E-01	1.00E+00	9.43E-01
Zr-93	4.04E-09	4.04E-09		
Zr-95	6.44E-04			
Nb-95m	6.14E-06			
Nb-94	1.75E-06	1.75E-06		
Nb-95	1.63E-03			
Nb-93m	6.19E-06	4.97E-05		
Mo-93	1.38E-04	1.38E-04		
Tc-99	1.31E-03	1.31E-03		

Table 3. Activities of specific radionuclides on concrete structures.

Activities of typical radionuclides on concrete

after 1000 shots

Volume (cm^3)	
Floor	1.75E+09
Wall & Ceiling	1.34E+10

radio-nuclides	Wall & Ceiling Concrete (Horizontal port model)		Floor Concrete (Vertical port model)	
	after 1year (Bq/cc)	after 10years (Bq/cc)	after 1year (Bq/cc)	after 10years (Bq/cc)
Be-10	8.08E-13	8.08E-13	3.76E-12	3.76E-12
C-14	2.16E-05	2.15E-05	8.18E-05	8.17E-05
Na-22	3.91E-05	3.56E-06	1.84E-04	1.68E-05
Al-26	2.58E-10	2.58E-10	1.22E-09	1.22E-09
Si-32	6.05E-13	6.00E-13	2.84E-12	2.81E-12
P-32	7.63E-10	5.99E-13	3.64E-09	2.81E-12
P-33	3.78E-08		1.88E-07	
S-35	1.36E-03		5.08E-03	2.80E-14
Cl-36	1.37E-07	1.37E-07	5.35E-07	5.35E-07
Ar-37	6.78E-04		3.28E-03	
Ar-39	2.57E-04	2.51E-04	1.25E-03	1.22E-03
K-40	8.58E-01	8.58E-01	8.58E-01	8.58E-01
Ca-41	1.67E-04	1.67E-04	6.24E-04	6.24E-04
Ca-45	3.68E-01	3.70E-07	1.37E+00	1.38E-06
Cr-51	2.12E-08		9.87E-08	
Mn-53	2.03E-11	2.03E-10	9.54E-11	9.54E-11
Mn-54	4.24E-04	2.87E-07	2.03E-03	1.37E-06
Fe-55	2.24E-01	2.19E-02	8.38E-01	8.21E-02
Fe-59	6.41E-04		2.45E-03	

Tables 2, 3 show results of the typical radionuclide densities on the stainless steel (SS-316) structures and concretes.

Two kinds of data, one-year interval and ten years interval after 1000 shots operation, were shown. In these tables, data less than 1.0×10^{-14} (Bq/cc) were omitted. Since neutron flux through the big vertical port gives strong contribution to the floor concrete, result of the vertical port model is shown for floor concrete. Others are results of the horizontal port model.

From one to ten years after 1000 shots operation, main radionuclides contributed to the γ-ray dose are ^{55}Fe (half-life of 2.73 y) and ^{60}Co (5.27 y) for structures of stainless steel, and ^{40}K (1.28×10^{9} y) and ^{55}Fe for concretes. However, almost of ^{40}K are natural nuclides existing in concrete.

5. Conclusions

In this paper, the 2-D neutron transport code DOT-3.5 and the induced radioactivity calculation code CINAC were employed to identify the radionuclides and to evaluate the dose rate during and after experimental series in LHD. Detailed analysis of activation properties and the dose rate for individual structural materials of LHD were carried out. Major results are as follows:

(1) In the SS-316 materials, dominant radionuclides just after shots are ^{56}Mn. Finally ^{60}Co becomes dominant.
(2) In concrete, dominant radionuclides just after shots are ^{24}Na. Although ^{40}K becomes dominant finally, it is almost natural nuclides.
(3) γ-ray dose rate decreases one order during weekend interval. This level of 10μSv/h is lower than the limitation for worker (20mSv/y) who works for 2000 hours per year.

References

[1] A. Iiyoshi, M. Fujiwara, O. Motojima, N. Ohyabu and K. Yamazaki, Fusion Technology **17**, 169 (1990).

[2] O. Motojima, K. Akaishi, M. Asao, K. Fujii *et al*., in Plasma Phys. and Contr. Nucl. Fus. Res 1990 (Proc. 13th Int. Conf. Washington DC, 1990), Vol.**3**, IAEA, Vienna, 513 (1990).

[3] A. Iiyoshi, A. Komori, A. Ejiri, M. Emoto *et al*., Nucl. Fusion **39**, 1245 (1999).

[4] M. Fujiwara, H. Yamada, A. Ejiri, M. Emoto *et al*., Nucl. Fusion **39**, 1659 (1999).

[5] H. Handa, K. Hayashi, Y. Ogawa, Y. Sakuma, H. Obayashi et al., Fusion Eng. Des. **17** 335 (1991).

[6] H. Handa, K. Hayashi, H. Yamanishi, Y. Sakuma, H. Kaneko et al, Fusion Eng. Des. **28** 515(1995).

[7] W.A. Rhoades, F.R. Mynatt, Tech. Memo. ORNL/TM-4280, Oak Ridge National Laboratory, Oak Ridge, TN, 1973.

[8] Fukumoto, J. Nucl. Sci. Technol., **23**, 97 (1986).

[9] K. Maki, K. Kosako, Y. Seki, H. Kawasaki, Rep. JAERI-M 91-072, Japan Atomic Energy Research Institute, June 1991.